Properties of Conductive Oxygen Vacancies and Compact Modeling of IV Characteristics in HfO_2 Resistive Random-Access-Memories

Junsung Park, Min-Jae Kim, Jae-Hyung Jang, and Sung-Min Hong
School of EECS, Gwangju Institute of Science and Technology, Gwangju, Republic of Korea
email: smhong@gist.ac.kr

***Abstract*—The HfO_2-based resistive random-access-memory (RRAM) is studied. In the first part, two parameters of oxygen vacancies are extracted. The migration barrier of the oxygen vacancy (or the extended Frenkel pair) is calculated. The resistivity of a filament is also calculated. In the second part, an existing compact model for the RRAM is implemented and its results are compared with the experimental data.**

I. Introduction

The resistive random-access-memory (RRAM) has been studied intensively. It has been regarded as a promising candidate for future non-volatile memory and neuromorphic applications. They show fast operation (nanosecond operation), scalability (scaling down to tens of nanometer), and multi-bit topology. Structural simplicity is another advantage of the RRAM devices.

It has been reported that various materials can be used as switching layers. Among them, especially, the HfO_2-based RRAMs are widely adopted, because it can be successfully integrated into the modern CMOS technology. From the viewpoint of power, stability, and operation speed, the HfO_2-based RRAM exhibits superior performance.

It is known that the conductive filament plays an important role in the HfO_2-based RRAMs. Shape of a filament, which is a conduction path made of oxygen vacancies, determines the electrical properties of the RRAM. Since the states are characterized by their resistance values, it is very important to understand the change of filament shape under a given operation condition. The modeling approach can be very helpful in this aspect.

In order to model the HfO_2-based RRAMs, various approaches with varying complexities (from the first-principles calculation to compact models) have been reported. For example, previous reports on the FEM/KMC approaches [1], [2] are available. Parameters are quite important in those device simulations. A systematic procedure to extract the related parameters is highly desirable.

In this work, properties of oxygen vacancies are calculated with the density-functional theory code (Vienna Ab initio Simulation Package, VASP [3], [4]). Moreover, a measured IV curve of a HfO_2-based RRAM is calculated by employing an existing compact model. The organization of this extended abstract is as follows: In Section II, the migration barrier of oxygen vacancies are calculated. In Section III, the resistivity of a HfO_2 supercell is calculated. In Section IV, an existing compact model is implemented and its results are compared with the experimental IV curve. The conclusion is drawn in Section V.

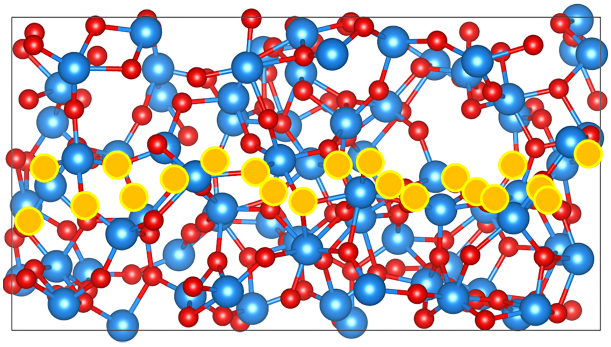

Fig. 1. One example of the atomistic structure of an amorphous HfO_2 system. Yellow dots represent the possible defect locations, considered in Fig. 2. In the actual calculation, several amorphous structures are generated.

II. Migration barrier of oxygen vacancies

The switching operation of the HfO_2-based RRAM is explained by the migration of oxygen vacancies. The migration barrier of oxygen vacancies, the difference between the local maximum and minimum formation energies, is an important material parameter to affect the vacancy migration.

In Fig. 1, an atomistic structure of an amorphous HfO_2 system is shown. The structure is obtained by the DFT-MD optimization. In the cell optimization, the PBEsol exchange-correlation functional is used. In addition to an amorphous structure, a tetragonal supercell structure is also considered. Each structure (amorphous or tetragonal) has 108 atoms.

After the atomic structure is prepared, a defect is introduced. Two defect types – an oxygen vacancy and the extended Frenkel pair, which is a pair of an oxygen vacancy and an oxygen interstitial – are considered. In the case of the tetragonal supercell, the defect is generated at each symmetric position inside a unit cell. However, for an amorphous structure, it is difficult to find symmetric positions. Therefore, we have manually selected possible defect locations as shown in Fig. 1.

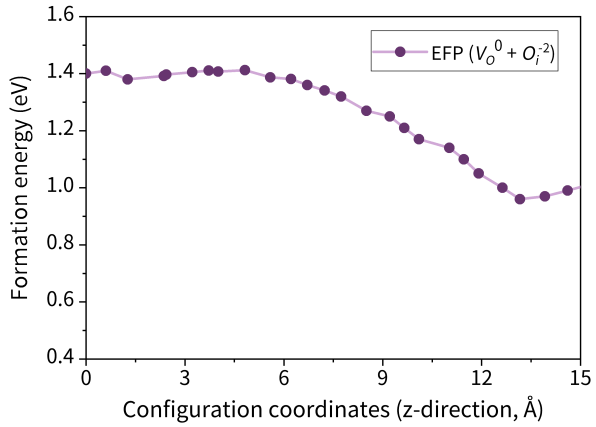

Fig. 2. Formation energy of the extended Frenkel pair for the structure shown in Fig. 1.

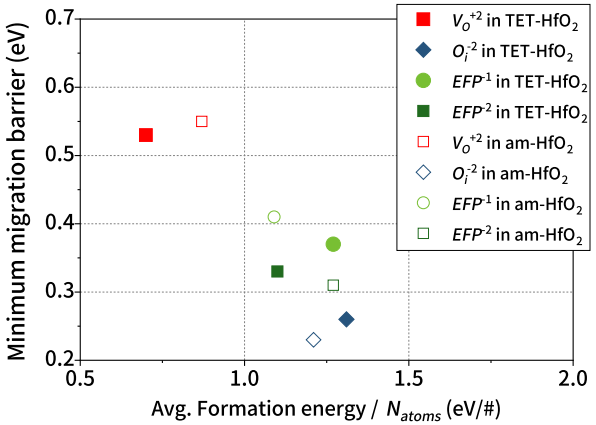

Fig. 3. Migration barriers of various defects in HfO_2. Both the crystalline and amorphous structures are considered.

At every defect position, the formation energy is calculated. When the formation energy is calculated, a hybrid exchange-correlation functional (optimized HSE) is used. The formation energy of the extended Frenkel pair [5] is drawn as a function of the position in Fig. 2. In this example, the extracted migration barrier is about 0.45 eV.

For several amorphous structures (5-10 samples), the same calculation has been performed in order to improve the fidelity. As stated above, the crystalline HfO_2 (the tetragonal structure) has been also considered for comparison. In Fig. 3, the results are summarized. The minimum value of the extracted migration barrier is reported. Filled symbols are results for the crystalline structure, while empty ones are results for amorphous structures. They exhibit good qualitative agreement. The extended Frenkel pair has a much lower migration barrier than the oxygen vacancy. An oxygen ion interstitial is lowering the migration barrier of the corresponding oxygen vacancy.

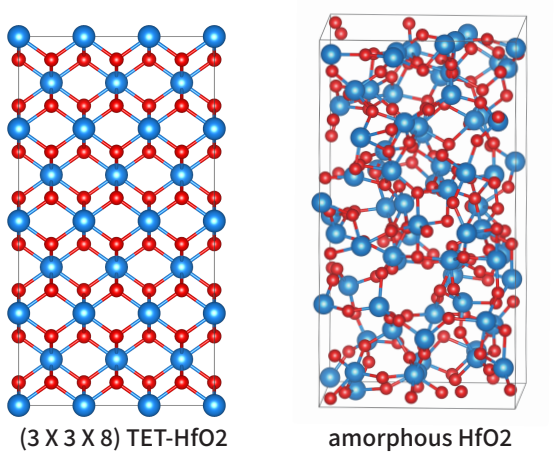

Fig. 4. HfO_2 supercells for the conductivity calculation. (Left) A crystalline structure and (Right) an amorphous structure.

III. Electrical Property of Oxygen Vacancy Filament

The migration barrier calculated in Section II is related with how the filament shape changes. On the other, when the filament shape is fixed at a given time instance, the conduction property is of interest.

The resistivity of a HfO_2 supercell is calculated. First, a structure is prepared. In Fig. 4, the atomistic structures are shown. Both the crystalline structure (the tetragonal structure with $3 \times 3 \times 8$ unit cells) and the amorphous one are considered. 296 atoms are included in each supercell. The procedure to generate a structure is similar with that in Section II.

Starting from these structures, oxygen vacancies are introduced to generate an oxygen vacancy filament. The resistivity along the vertical direction is calculated with the Mott formula [6]. The conductivity tensor is obtained by using the linear response function of the VASP package. The k-point sampling is done with a $4 \times 4 \times 20$ grid. In Fig. 5, the energy spectrum of the calculated conductivity is drawn for HfO_2 nanorods. In the case of a defect-free crystalline system, it is an insulator because no contribution in the forbidden zone. On the other hand, when defects are introduced, the defect states in the forbidden zone significantly contribute to the conductivity.

In Fig. 6, the resistivity is drawn as a function of the defect density. Each symbol represents a distinct sample. Amorphous samples have relatively higher resistivity that the crystalline ones. When the number of oxygen vacancies increases from 2 to 8, the resistivity of the crystalline HfO_2 increases almost six orders-of-magnitude. Similar trends are found for different samples. Since the atomistic simulation model is much limited in its size (0.8 nm $\times$ 0.8 nm $\times$ 1.5 nm), the defect density is unrealistically high. A direct comparison with the experimental results is not possible. Instead, in the right subfigure of Fig. 6, the experimental results in previous reports [1], [2] are drawn with their original defect density without scaling. A good qualitative agreement is obtained.

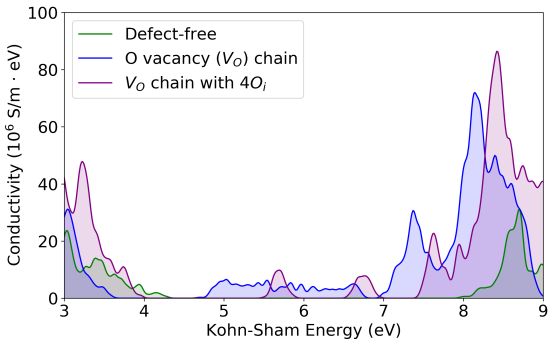

Fig. 5. Energy spectrum of the calculated conductivity of HfO_2 nanorods. The x-axis is Kohn-Sham energy.

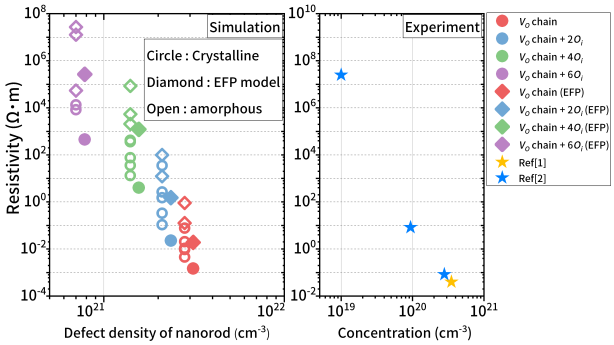

Fig. 6. (Left) Calculated resistivities of various HfO_2 structures. When the number of oxygen vacancies increases, the resistivity decreases exponentially. (Right) Experimental results in [1], [2].

IV. Compact Modeling of IV Characteristics

A HfO_2-based RRAM is fabricated. A 90-nm-thick SiO_2 layer is made on top of the p^+ silicon substrate. After the Ti/Pt (10/100 nm) bottom electrode is formed, the switching layer (HfO_2 15 nm) is deposited. The Ti/Pt (30/100 nm) layer acts as the top electrode. The top electrode has a circular shape and its diameter is 300 μm. In Fig. 7, the IV characteristics of a HfO_2-based RRAM measured at room temperature is shown. The compliance current is 10 mA. The SET and RESET voltages are 2.5 V and -1.1 V, respectively.

By adopting an existing compact model reported in [7], switching behaviors are calculated. In this model, the filament shape is simply characterized by a gap between the top electrode and the filament end point. The model equations are not repeated here and the interested readers are referred to [7]. The compliance current is implemented with an ideal MOSFET in the saturation mode. As shown in Fig. 8, it is shown that the compact model with adjusted parameters can reproduce the SET and RESET voltages considerably well.

Based on the calibrated compact model, the switching behaviors are predicted at various temperatures (down to 250 K), as shown in Fig 9. For lower temperatures, the absolute values of the SET and RESET voltages increase. A similar trend can be found in a previous report [8]. Sensitivities of the SET/RESET voltages with respect to the temperature are 0.5 V / 50 K and -0.36 V / 50 K, respectively.

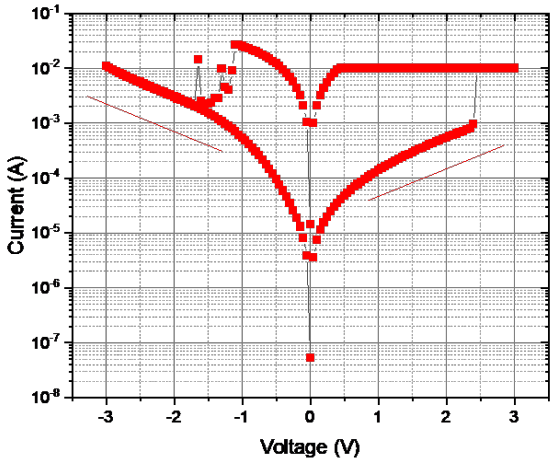

Fig. 7. Measured IV switching characteristics of a HfO_2-based RRAM. Thickness of the HfO_2 layer is 15 nm. The SET and RESET voltages are 2.5 V and -1.1 V, respectively.

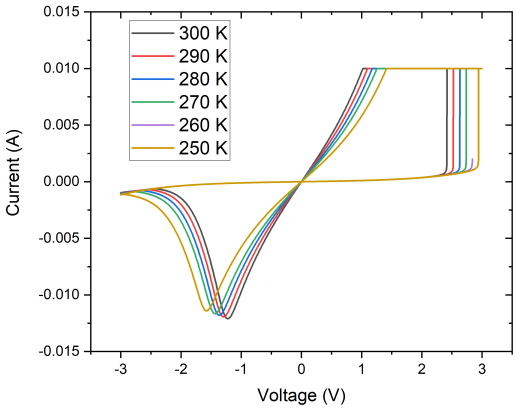

Fig. 8. Simulated switching characteristics of a HfO_2-based RRAM at various temperatures.

V. Conclusion

In summary, our recent research efforts on the HfO_2-based RRAM are presented. The material modeling (in Sections II and III) and the compact modeling (in Section IV) presented in this work will be combined with the FEM/KMC approaches to construct a fully functional modeling environment for the RRAM.

Acknowledgement

This work was supported by the National Research Foundation of Korea (NRF) grant funded by the Korea government (NRF-2019R1A2C1086656) and Samsung Electronics.

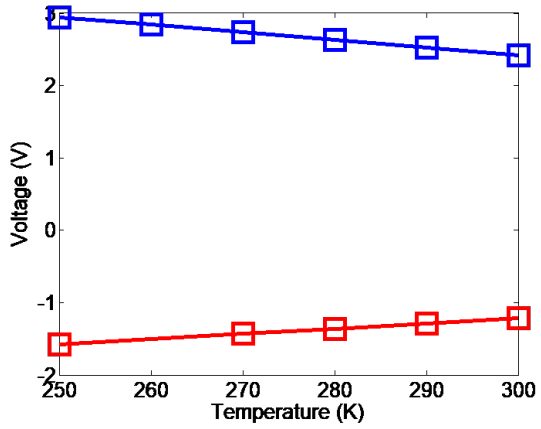

Fig. 9. SET (Blue) and RESET (Red) voltages of the RRAM in Figs. 7 and 8 as functions of the temperature.

REFERENCES

[1] S. Ambrogio, S. Balatti, A. Cubeta, A. Calderoni, N. Ramaswamy, and D. Ielmini, "Statistical fluctuations in HfOx resistive-switching memory: Part I - Set/Reset variability," *IEEE Transactions on Electron Devices*, vol. 61, no. 8, pp. 2912–2919, 2014.

[2] A. Padovani, L. Larcher, O. Pirrotta, L. Vandelli, and G. Bersuker, "Microscopic modeling of HfOx RRAM operations: From forming to switching," *IEEE Transactions on Electron Devices*, vol. 62, no. 6, pp. 1998–2006, 2015.

[3] G. Kresse and J. Hafner, "Ab initio molecular dynamics for liquid metals," *Phys. Rev. B*, vol. 47, pp. 558–561, Jan 1993. [Online]. Available: https://link.aps.org/doi/10.1103/PhysRevB.47.558

[4] ——, "Ab initio molecular-dynamics simulation of the liquid-metal–amorphous-semiconductor transition in germanium," *Phys. Rev. B*, vol. 49, pp. 14 251–14 269, May 1994. [Online]. Available: https://link.aps.org/doi/10.1103/PhysRevB.49.14251

[5] B. Traoré, P. Blaise, and B. Sklénard, "Reduction of monoclinic HfO_2: A cascading migration of oxygen and its interplay with a high electric field," *The Journal of Physical Chemistry C*, vol. 120, no. 43, pp. 25 023–25 029, 2016.

[6] S. J. Blundell and K. M. Blundell, *Concepts in Thermal Physics*. OUP Oxford, 2009.

[7] P. Chen and S. Yu, "Compact modeling of RRAM devices and its applications in 1T1R and 1S1R array design," *IEEE Transactions on Electron Devices*, vol. 62, no. 12, pp. 4022–4028, 2015.

[8] R. Fang, W. Chen, L. Gao, W. Yu, and S. Yu, "Low-temperature characteristics of HfOx-based resistive random access memory," *IEEE Electron Device Letters*, vol. 36, no. 6, pp. 567–569, 2015.